# Fate and Transport of Seacliff Failure Sediment in Southern California

Authors: Olsen, Michael J., Johnstone, Elizabeth, Driscoll, Neal, Kuester, Falko, and Ashford, Scott A.

Source: Journal of Coastal Research, 76(sp1) : 185-199

Published By: Coastal Education and Research Foundation

URL: https://doi.org/10.2112/SI76-016

| Journal of Coastal Research | SI | 76 | 185–199 | Coconut Creek, Florida | 2016 |
|---|---|---|---|---|---|

# Fate and Transport of Seacliff Failure Sediment in Southern California

**Michael J. Olsen[†*], Elizabeth Johnstone[‡], Neal Driscoll[‡], Falko Kuester[‡], and Scott A. Ashford[†]**

[†]School of Civil and Construction Engineering
Oregon State University
Corvallis, OR 97331, U.S.A.

[‡]Scripps Institution of Oceanography
University of California, San Diego
La Jolla, CA 92093, U.S.A.

www.cerf-jcr.org

www.JCRonline.org

## ABSTRACT

Olsen, M.J.; Johnstone, E.; Driscoll, N.; Kuester, F., and Ashford, S.A., 2016. Fate and transport of seacliff failure sediment in southern California. *In*: Brock, J.C.; Gesch, D.B.; Parrish, C.E.; Rogers, J.N., and Wright, C.W. (eds.), *Advances in Topobathymetric Mapping, Models, and Applications*. *Journal of Coastal Research*, Special Issue, No. 76, pp. 185–199. Coconut Creek (Florida), ISSN 0749-0208.

Continual erosion and collapse of unstable seacliffs along the economically important coastline of San Diego County, California, threatens existing development and public safety. Frequent time-series mapping of the seacliffs and beaches provides valuable insight into the processes responsible for cliff erosion and into the reworking and transport of the failed material. High-resolution terrestrial laser scan (TLS) data provide quantitative data for analyzing seacliff morphology, capturing patterns over time and across a wide range of spatial scales. Through an ongoing "rapid response" program operational since spring 2007, eleven substantial seacliff failure sites were mapped pre-collapse, immediately post-collapse, and repeatedly after the collapse to constrain processes causing cliff failure and estimate the rate at which failed material is reworked. Comparison of the TLS data with water levels and climate data highlights the contributing mechanisms to the seacliff failures and the rapid reworking of the failed material. Failure sites were categorized based on the frequency of wave contact (*i.e.*, total water level) compared with the beach elevation to assess differences in the rates of sediment reworking. For example, unconsolidated failed material on the beach was reworked quickly by waves at sites where waves reached the failure on a nearly daily basis. Conversely, other failure masses with less wave contact were only reworked during storm events producing larger waves. At sites where the failure material consisted of large boulders, there are feedback mechanisms at play where the failed material protects the cliff toe by stabilizing talus deposits, akin to riprap engineering techniques. Failures due to wave undercutting and notching were observed to migrate laterally at these sites. This lateral progression of failures might explain the long-term linear retreat of the seacliffs in the region, which minimizes the development of embayments and promontories.

**ADDITIONAL INDEX WORDS:** *Sediment transport, seacliff erosion, terrestrial laser scanning, lidar.*

## INTRODUCTION

Several mechanisms contribute to the destabilization of seacliffs (Benumof *et al.*, 2000; Sunamura, 1992; Wolters and Muller, 2008). While seacliff erosion threatens development and infrastructure built on the coastline (Griggs *et al*., 2005), this necessary and natural process provides vital sediment to the beach (Haas, 2005; Young and Ashford, 2006). Subaerial erosion breaks up the cliff from the top down and tends to relax or diminish the slope (Weissel and Driscoll, 1998). Chemical weathering caused by carbonic and humic acids dissolves the weakly cemented sandstone, which increases surface roughness and irregularities in the cliffs. Wave-induced erosion tends to create notches at the base of the cliff and creates vertical cliff faces when failures occur from wave undercutting. A spatially more linear form of seacliff retreat is observed. Dong and Guzzetti (2005) determined that seacliff erosion rates tend to slow after larger failures and discussed the need for more high-resolution data to compare the contribution of large and small events to sediment budgets. Young *et al*. (2009) studied the interdependence and contributions of both waves and precipitation in eroding seacliffs in southern California using airborne lidar data surveys acquired at 6-month intervals.

Most prior research has been concerned with the volume of material released from the cliff and overall rate of erosion (*e.g.*, Hapke and Richmond, 2000; Moore *et al*., 1999). This research builds on these and other previous efforts to document and analyze erosional processes at a finer temporal and spatial scale. In particular, the rate at which material is reworked from the cliff to the beach (or other locales) has not been documented with sufficient temporal resolution. The fine temporal and spatial resolution of this dataset provides insights on the sequencing of failures across the cliff face and illustrates how liberated material is quickly reworked by wave action, even during low energy periods such as the summer.

While this research represents a short time series in a geologic sense, it is the start of a long-term study that has only recently become possible with advances in geomatics technologies. A longer term dataset is necessary to analyze the cumulative contributions of small events over time and establish overall erosion rates. Hence, the intent of this paper is not to draw any long-term conclusions. Much valuable information about

*DOI: 10.2112/SI76-016 received 13 January 2015; accepted in revision 28 October 2015.*
*Corresponding author: michael.olsen@oregonstate.edu

erosion and reworking, however, can still be gleaned within a short time window with fine temporal resolution that is not often captured in longer term studies.

**Technological Background**

Several methods for analysis of seacliff retreat such as digital photogrammetry (*e.g.*, Hapke and Richmond, 2000; Moore *et al*., 1999), aerial light detection and ranging (lidar) (*e.g.*, Young and Ashford, 2006; Young *et al*., 2009), and oblique helicopter lidar (Rosser *et al*., 2008) have yielded important results, yet they have limitations for repeated coastal cliff surveys due to logistics, mobilization expense, lower spatial and temporal resolution, and/or the ability to capture the cliff face topography (including complex sea caves) in sufficient detail (Young *et al*., 2010a). In order to document the reworking processes of interest, the corresponding data must be regularly obtained at finer temporal scales before being overprinted by other events.

Terrestrial lidar (also known as terrestrial laser scanning, TLS) has been proven to be an effective tool to study seacliff failures and morphology (Collins and Sitar, 2004; Collins *et al*., 2007; Lim *et al*., 2005; Rosser *et al*., 2005; Young and Ashford, 2007). TLS uses time-of-flight or phase-based measurements to determine the distance of a sample point. TLS captures topological characteristics at high resolution, producing a detailed point cloud containing XYZ coordinates, RGB color, and return signal intensity information. A single scan with the I-Site 4400 scanner used for this study can acquire approximately 0.5–1 million sample points on the cliff and beach in about six minutes, densely (~100 points per $m^2$) covering about 70 m of coastline, depending on the complexity of the topography and efficiency of the surveyors. Multiple scans are registered together in order to produce a continuous topographic model of the coastline.

The aforementioned studies using TLS have proven the effectiveness of TLS to capture geometry for high-resolution 3D modeling at a limited temporal resolution. This study builds upon previous work and reveals additional insights obtained through a "rapid response" program (Olsen *et al*., 2008) with repeated mapping of a large (~20 km) section of coastline supplemented with more frequent scans at sites after a failure occurs to track the dispersion of failure sediment. As the coastal environment is dynamic, continual observation is necessary to understand and assess coastal change.

**Regional Setting**

This study focuses on seacliff erosion and failure along the northern portion of San Diego County from Scripps Pier to Batiquitos Lagoon in Encinitas covering ~20 km of coastline (Figure 1). The study area is divided into several sections based on natural breaks in the seacliffs by lagoons or canyons: Scripps, Black's Beach, Torrey Pines, Del Mar, Solana Beach, and Encinitas. Cliff heights typically vary from 20–100 m in height throughout the study area. Young *et al*. (2010b) present detailed cliff height maps across the study area. The coastline is heavily urbanized with the exception of the Torrey Pines section, which is a State Reserve. This development has created increased surface runoff and groundwater from urban landscaping and irrigation. Vegetation also covers the tops of many cliffs. Most of the lower portion of the cliffs of the Solana Beach section are armored with seawalls or other stabilization techniques.

The coastal sediments of San Diego County consist of several well-sorted, cemented marine terraces that have formed as a result of sea level rise and fall in combination with tectonic activity throughout California's geologic history (Kennedy, 2005). Miocene and Eocene deposits include nearshore marine, beach, estuarine, lagoonal, and continental dune facies that have undergone cementation and compaction. A geologic map of the cliffs in the study area is presented in Young *et al*. (2009).

Two major geologic formations within this study are the Delmar Formation and the Torrey Formation, both deposited during the Eocene epoch. The Delmar Formation is composed of fine-grained clays and silts with occasional sands deposited in an estuarine lagoonal environment. Strongly cemented shells within the cohesive clay make the Delmar more resistant to erosion than the overlying Torrey Formation. The Torrey Formation consists of weakly-cemented, coarser-grained sandstone from barrier beach deposits formed along a submerging coastline (Kennedy, 1973). The cementing allows the cliffs to stand near-vertical. However, when meteoric water permeates the sandstone, the cement is dissolved and the sandstone begins to crumble. Wind erosion accentuates these areas of differential erosion and produces an alveoli (*i.e.*, honeycomb) morphology.

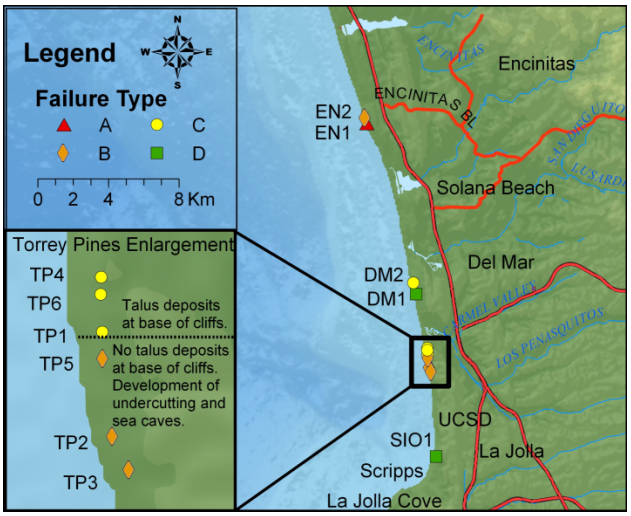


Figure 1. Study area map with locations of failure sites. Note the demarcation line between cliffs with and without talus deposits. Type C failures occurred from subaerial erosion in areas with talus deposits on the north, and Type B failures occurred to the south from wave undercutting because of no protective talus deposits. (Failure types are defined in Figure 6.)

San Diego has a Mediterranean type climate with little rainfall throughout the year (NOAA, 2008a), especially during the summer months. Precipitation and wave intensity vary significantly between El Niño (warm), La Niña (cold), and Pacific Decadal Oscillation (PDO) weather patterns. Young *et al*. (2009) present an overview of precipitation and wave heights

typically experienced near the study area. This study was performed during a relatively dry period with typical wave activity.

## METHODS

Several data sources were required to assess change at each of the failure sites studied. First, TLS was used to create models of the seacliff and failure mass geometries. Changes in geometric conditions were assessed by determining failure volumes and evaluating changes in beach elevation. These geometric changes were compared to environmental data observed near the sites to understand potential failure triggers. Based on the environmental data, the failure sites were then classified based on differences in wave contact frequency. The methodology for each of these analysis steps will now be discussed in detail.

### TLS Surveying

Regional baseline scans were performed at least twice a year (more frequently in high priority areas) to quantify seasonal variability. Lifeguards, state park officials, and volunteers helped to quickly identify new seacliff failure sites. Sections of the study area were prioritized for baseline surveys by considering the most recent observations of failures dispersed throughout the study area. For example, the Torrey Pines section was marked as the highest priority because of multiple observed collapses and scanned most frequently (4–6 times per year).

In addition to these larger regional surveys, specific site investigations (typically with a TLS) were performed as soon as possible (*e.g.*, within a day or two depending on tide constraints) after a seacliff failure to obtain accurate failure mass volumes before wave reworking. Table 1 provides a summary of the sites, initial survey dates, and their environmental conditions. Additional site visits were conducted until the failure mass had more or less reached an equilibrium state.

The methods used to obtain and georeference these surveys to UTM Zone 11 (NAD 1983) coordinates are discussed in Olsen *et al*. (2009 and 2011). An I-Site 4400 laser scanner (I-Site, 2009) with an RTK GPS system was used for the survey work. Detailed, triangulated surface models used for volumetric analysis were created using the methodology described in Olsen *et al*. (2013). Additional point cloud and surface model processing and analysis was completed in Maptek I-Site Studio software (I-Site, 2009).

Because of the quantity and magnitude of surveys performed herein, only typical accuracies are reported. 3D RMS differences in measurements on the unchanged portions on the cliff were typically 6–8 cm between surveys. Volumetric error estimates were typically below 10%. Sample point spacings were generally between 4–8 cm on the cliff face. In addition to periodic surveys, frequent photographic surveys also were performed, enabling the research team to bracket failure dates.

### Calculating Failure Mass Volumes

A comparison of 3D cliff surface models can determine the initial volume of the failure mass. This calculated volume can be compared to the failure mass measured on the beach. However, caution must be used in the algorithm used to calculate the volume because it should be orthogonal to the cliff for best results. If an algorithm performs the calculation by a look in the Z (nadir, elevation) direction toward the XY (Northing-Easting horizontal) plane, the volume can be erroneous if there is an overhang in the cliff because it may not be accounted for in the volumetric analysis using the horizontal plane for reference. Rapid response after the failure ensures that the volumes calculated from the failure mass and the volume of sediment lost from the cliff should be nearly equivalent. Often because the failure is broken up with voids between blocks, it can have a larger volume than that calculated from the cliff measurement. Additionally, if waves have reached the failure, its volume on the beach may not agree with the volume derived by differencing the seacliffs. These discrepancies are observed and will be discussed at a few sites discussed herein.

For this study, failure volumes were not differentiated between soil type and size to determine whether the sediments would remain on the beach during beach sorting processes. However, Young *et al*. (2010b) present research indicating that 80% of the sediments in the cliff are medium to coarse sand (Everts, 1990; littoral cutoff diameter > 0.06 mm), which can contribute to beach accretion.

Volumetric analysis in dynamic beach environments requires a systematic approach to calculate failure mass volumes. Depending on site morphology, different methods need to be implemented to produce consistent results. The methods used for creating a baseline surface of the beach for volume calculations are illustrated in Figure 2A and vary depending on the site profile and if previous failures have occurred at the site. These methods assume that unless the failure mass is on an unchanging platform, all failure mass volumes are determined relative to the current surrounding beach level. Thus, any sediment derived from the failure mass that is below the current beach datum becomes part of the beach and no longer is considered part of the failure mass volume.

### Modeling Beach Elevation Change

Beach elevations obtained from the TLS data were plotted for the seaward edge ($E_{B0}$, Figure 2B) of each failure site to determine the frequency of waves reaching the failure mass. Additionally, where available, beach elevations at locations 5 m, 10 m, 15 m, and 20 m directly seaward of the failure mass are overlain on plots of the total water level with time. These measurement locations are determined relative to the original failure location and held fixed as the failure mass erodes so that representative fluctuations in beach elevation can be observed.

In addition to $E_{B0}$, the maximum failure mass elevation is also recorded for each TLS survey. As the failure mass is eroded and reworked by waves, the crest of the failure mass is lowered, eventually becoming part of the typical beach profile. However, the beach generally slopes upward toward the east. Hence, the beach elevations obtained at the edge of the failure mass will typically be lower than the beach elevation directly below other locations within the failure mass.

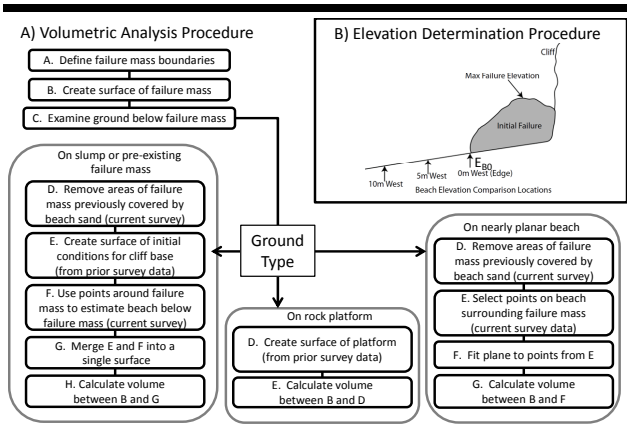


Figure 2. (A) Workflow for the calculation of failure mass volume depending on site geometry. (B) Schematic of elevation measurement locations for beach elevation and maximum failure mass elevation. Note that the measurement locations for beach elevation are measured relative to the edge of the initial failure mass and are held constant as the failure mass erodes.

## Environmental Conditions

Environmental conditions are critical to understand seacliff erosion and the integration of sediments derived from cliff failures. Of note, the quantity, intensity, and frequency of precipitation and inundation (total water level based on wave heights and tidal data) are especially important for understanding failure mechanics. For this study, precipitation data were obtained from NOAA station 23188 (NOAA, 2008a) at the San Diego Airport. Although hourly precipitation information is available, daily summaries were used for the analysis given the limited ability to resolve the time of failure as well as the relative infrequency of rainfall in San Diego.

Wave height, period, and directional information were obtained from the Coastal Data Information Program (CDIP) deepwater buoy 100 (Torrey Pines Outer, Scripps, 2008), which is located approximately 12 km offshore from Torrey Pines beach. The water depth is approximately 550 m at this station. While this station is far from shore, closer stations were not available, and the empirical relations used for runup calculations use deep-water parameters. To fill a data gap from buoy 100 during the period between December 5, 2007, and December 12, 2007, data from the Mission Beach (station 93) and Oceanside (station 45) buoys were averaged to estimate wave heights for the missing time period. A comparison of these datasets for December exhibits reasonable agreement (Olsen, 2009).

The runup level (Figure 3) can then be estimated using the following empirical equation (Stockdon *et al*., 2006), developed using deep-water parameters:

$$R_{2\%} = 1.1\left(0.35\beta(H_O L_O)^{1/2} + \frac{[H_O L_O(0.563\beta^2+0.004)]^{1/2}}{2}\right) \quad (1)$$

where $R_{2\%}$ = the wave runup elevation with a 2% probability of exceedance, $\beta$ = the foreshore beach slope, $H_O$ = the deepwater wave height, and $L_O = (g/2\pi)T^2$ = the deepwater wavelength, where $T$ = the peak spectral wave period, and $g$ = the acceleration of gravity (9.807 m/s$^2$). A typical beach slope of $\beta$ = 0.05 was used, which was determined based on several TLS surveys throughout the study area ($\sigma$ = 0.015).

Tidal information was obtained from the NOAA tidal gage 9410170 (NOAA, 2008b) and converted to NAVD88, which is the same vertical datum used for the TLS data. The tidal data were then added to the calculated wave runup to derive an estimate of the total water level (TWL) using the method outlined in Ruggiero *et al*. (1996; 2001) and Ruggiero (2008), enabling comparison of the TWL to the measured beach and failure mass elevations. Erosion of the failure mass occurs with wave contact when the TWL exceeds the elevation of the beach at the seaward edge of the failure mass.

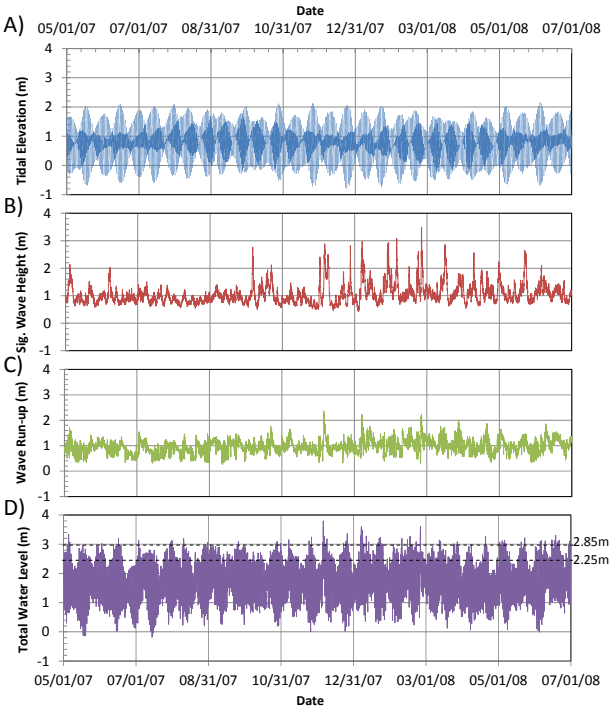


Figure 3. Calculation of Total Water Level (NAVD88) using the method described in Ruggiero (2008) from (A) Tidal measurements (NOAA Station 9410170), (B) Significant Wave Height (CDIP buoy TP100), (C) Wave Runup with 2% proabability of exceedance (calculated using Stockdon, 2006) producing (D) a total water level estimate.

## Failure Site Classification Scheme

Photographs of each failure site are presented in Figure 4. Site characteristics including estimated date of failure, volume, and presence of talus can be found in Table 1. Figure 5 compares each failure occurrence date with the environmental conditions including precipitation and total water level. This comparison provides a general insight into the potential factors that may have contributed to the failure.

The failure sites were divided into four major categories (Figure 6) based on frequency of wave contact by comparing TWL with beach elevation at the seaward edge of the failure mass, $E_{B0}$. The classification was developed to assist in the prioritization of sites for repeat surveys and to understand sediment redistribution patterns. This classification is a function of the beach attributes such as elevation, profile, and typical beach width. Although there is some variance in beach width in the study area, most beaches are relatively narrow (approximately 50–70 m wide at low tides during summer months). These classifications were created as follows:

(A) TWL frequently exceeds $E_{B0}$, resulting in consistent wave contact on a nearly daily basis (Sites: EN1). These sites occur in areas where the waves directly impact the cliff regularly throughout the year and thus would typically be wave-induced failures. The sediment from these sites is quickly reworked and distributed along the beach. These sites are where $E_{B0}$ is typically lower than the mean TWL plus one standard deviation (2.25 m).

(B) TWL periodically exceeds $E_{B0}$, resulting in intermittent wave contact on a weekly to monthly basis (Sites: EN2, TP2, TP3, TP5). This contact is often during very high tides or minor storm events. Failures typically occur as a result of wave-induced erosion processes. At these sites, $E_{B0}$ is typically larger than the mean plus one standard deviation (2.25 m), but lower than the mean TWL plus two standard deviations (2.85 m for the study period).

(C) TWL occasionally exceeds $E_{B0}$, resulting in infrequent and/or seasonal wave contact (Sites: TP1, TP4, TP6 and DM2). These sites experience wave contact very infrequently (*e.g.*, only during large winter storms or extreme high tides) because of protection offered by either

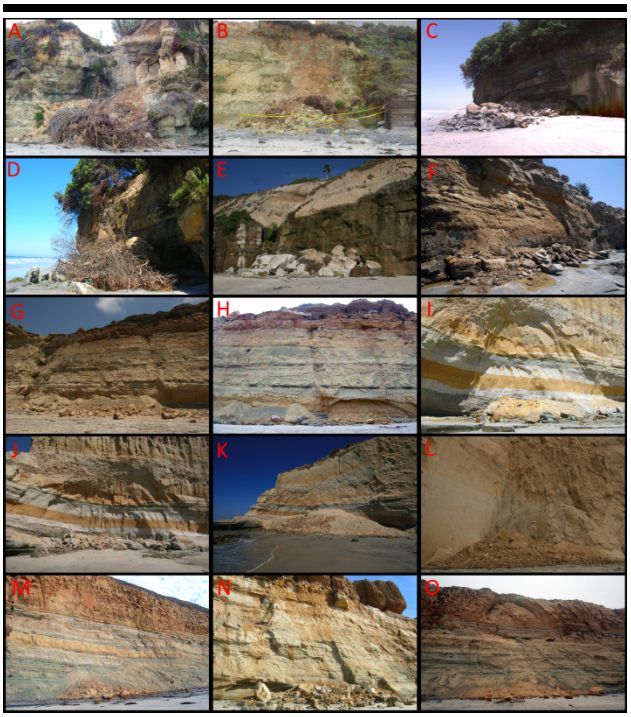


Figure 4. Photographs of failure sites (A) **DM1** 8/24/2008 (B) **DM2** 8/24/2008 (C) **EN1** a 6/7/2007 (D) **EN1b** after second failure 9/10/2007 (E) **EN2** 3/7/2008 (F) **SIO1** 9/25/2007 (G) **TP1a** 8/6/2007 (H) **TP1b** after second failure 7/8/2008 (I) **TP2a** 9/10/2007 (J) **TP2b** after second failure 3/4/2008 (K) **TP2c** after third failure 10/2/2008 (L) **TP3** 10/14/2007 (M) **TP4** 10/29/2007 (N) **TP5** 1/31/2008, and (O) **TP6** 6/18/2008.

Table 1. *Summary of failure sites and environmental conditions at failure (Geologic Units: DM = Delmar and TS = Torrey Sandstone formation).*

| Site | Type | Geologic Unit | Failure Date | Initial post-failure survey date | Initial Failure Vol. ($m^3$) | Talus Deposits | Environmental factors: High Water | Environmental factors: Ground-water | Environmental factors: Precip. | Probable cause of failure |
|---|---|---|---|---|---|---|---|---|---|---|
| EN1a | A-SL | DM | 6/6/2007 | 6/7/2007 | 139 | N | Y | Y | N | Undercutting/Groundwater |
| EN1b | A-S | TS | Sept 2007 | 9/10/2007 | 30 | N | Y | Y | N | Retrogressive failure |
| EN2 | B-L | DM | Feb 2008 | 3/7/2008 | 177 | N | Y | Y | N | Undercutting/Groundwater |
| TP1 | C-M | TS | 8/4/2007 | 8/6/2007 | 31 | Y | N | N | N | General Instability |
| TP2a | B-M | TS | 8/23/2007 (±1 day) | 8/24/2007 | 79 | N | Y | N | N | Undercutting |
| TP2b | B-M | TS | 2/10/2008 (±5 days) | 2/17/2008 | 50 | N | Y | N | N | Undercutting |
| TP2c | B-S | TS | 9/22/2008 | 9/23/2008 | 445 | N | Y | N | N | Retrogressive |
| TP3 | B-S | TS | 9/30/2007 (± 3days) | 10/5/2007 | 28 | N | Y | N | N | Wave impact |
| TP4 | C-M | TS | 10/20/2007 (±5 days) | 10/29/2007 | 168 | Y | Slight | N | Y | Precipitation |
| TP5 | B-M | TS | 1/28/2008 (±1 day) | 1/31/2008 | 120 | N | Y | N | Y | Precipitation |
| TP6 | C-M | TS | 6/16/2008 (±1 day) | 6/18/2008 | 77 | Y | Y | N | N | Bioerosion/ General Instability |
| DM1 | D-S | TS | 8/21/2007 (±7 days) | 8/28/2007 | 88 | N | N | Y | N | Groundwater |
| DM2 | C-S | TS | Summer 2007 | 8/28/2007 | 24 | N | N | Y | N | General Instability |
| SIO1 | D-M | TS | 9/2/2007 (±7 days) | 9/12/2007 | 30 | N | N | Y | N | Groundwater |

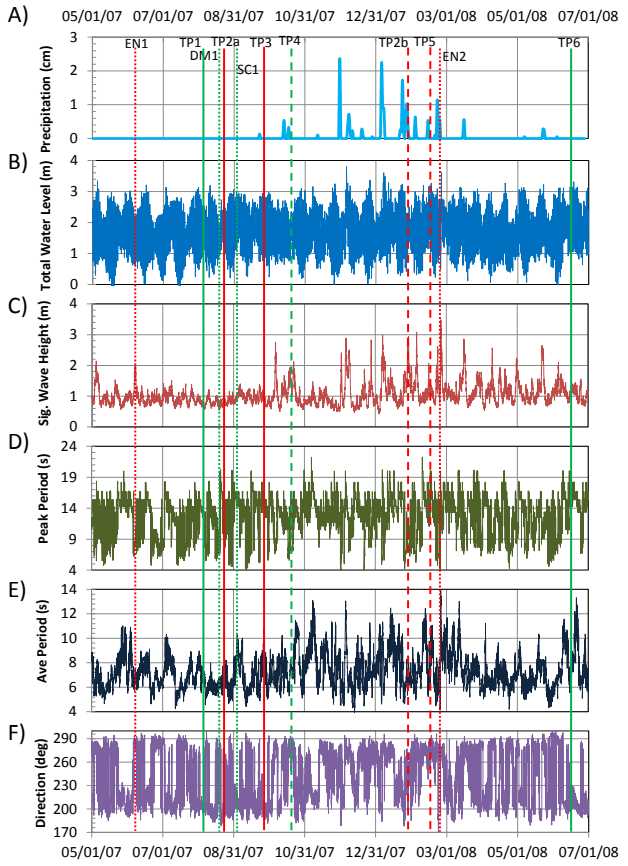


Figure 5. Comparison of failure occurrences with (A) precipitation (NOAA, Station 23188), (B) total water level, (C), significant wave height, (D) peak wave period, (E) average wave period, and (F) wave direction from CDIP buoy 100. Red lines denote predominantly wave-induced failures and green lines denote subaerial dominated failures. Dashed lines indicate that significant precipitation occurred close to the time of failure and dotted lines indicate the presence of groundwater at the site. Dates and times are Coordinated Universal Time (UTC).

a beach berm or a short rock platform during summer. Type C sites are also areas characterized by $E_{B0}$ higher than the mean TWL plus two standard deviations. These sites exhibit little to no change in failure mass volumes, with the only measurable changes taking place during larger storm or tidal events when the wave runup is large enough to reach the failure mass. These failures are, for the most part, caused by subaerial processes, although they can occur as a result of extreme wave events.

(D) TWL rarely exceeds $E_{B0}$, resulting in wave contact only when major storms or abnormal conditions occur (Sites: DM1 and SIO1). Type D sites have rare contact with waves, if at all, because the failure mass falls on an elevated rock platform. These failures are predominantly caused by subaerial processes.

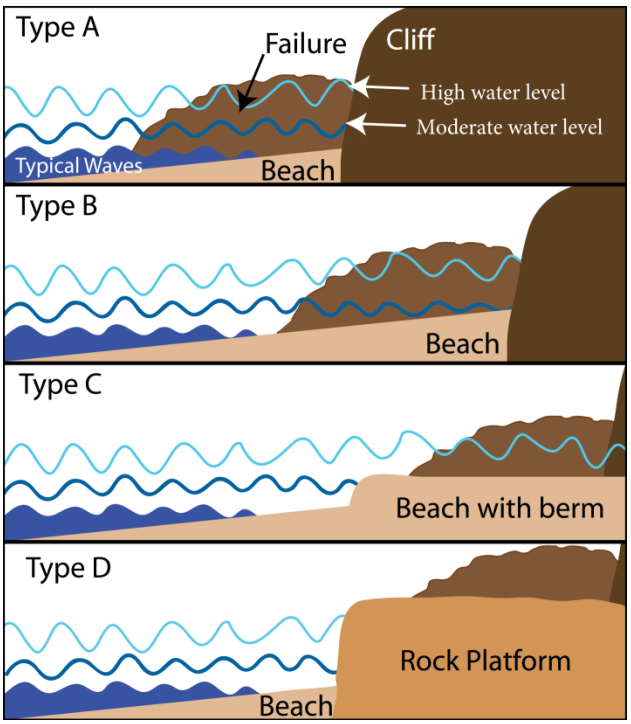


Figure 6. Comparison of typical site profiles at time of failure and varying wave conditions experienced at the site.

In addition to the classification based on TWL, a secondary identifier describing the dominant failure material size was utilized in Table 1, as follows:

S = mostly small-grained particles (sands, gravels, small clasts, and boulders up to 0.1 m in diameter)
M = mostly medium-sized clasts and boulders up to 0.3 m in diameter
L = mostly large clasts and boulders > 0.3 m in diameter.

The material size plays a significant role in determining whether it will be reworked by waves because failures with larger boulders and clasts will require much higher wave energy to be reworked.

## RESULTS

Failure site types A–D (Figure 6) were all observed throughout the study area. The individual sites are discussed (Figure 1, Figure 4) in light of failure type and rate of reworking, as well as relevant observations from the field investigations.

### Type A Failure Sites

#### EN1

This failure (Figure 4C, Figure 7) occurred on June 6, 2007, as a result of cliff collapse caused by a combination of wave undercutting creating a large sea cave and a substantial amount

of groundwater sapping. The timing of the failure correlates with frequent water contact at the cliff base (Figure 5). Groundwater expulsion occurs along the contact between the Del Mar and Torrey formations, because the claystone acts as an aquitard and thus creates a region of dense vegetation. The groundwater both added weight to the overhanging sandstone above the sea cave and weakened the sandstone by dissolving cements (Figure 8).

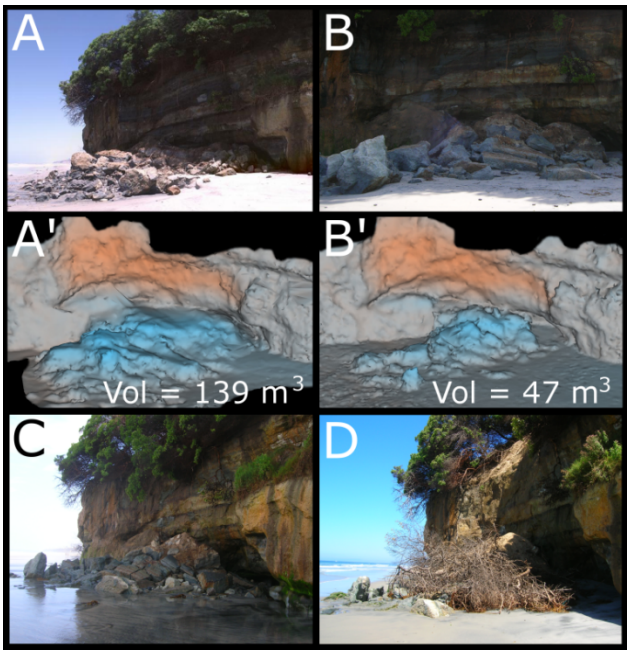


Figure 7. Surface comparison of a cliff failure in Encinitas (A) 6/7/2007 (1 day after) and (B) 6/22/2007 (2 weeks after). Lidar scans on the same dates are provided in (A') and (B') where blue represents accretion and orange represents erosion compared to scans from April 2005. Continual monitoring of the failure mass (C) from a site visit (7/28/2007) capturing the failure mass inundated from the waves, and (D) after collapse of vegetation above (9/10/2007).

This failure mass was continually impacted by waves (both summer and winter) except during low tides (see comparison of TWL to $E_{B0}$ in Figure 9). Volumetric analysis for the failure site (Figure 7 and Figure 9) highlights the impact of this frequent water contact on the slide mass. When scanned on the day after failure, the slide volume was 139 $m^3$. (The original volume was most likely larger as it was exposed to waves for a day.) Within two weeks of the failure (Figure 9), the slide volume dropped to 47 $m^3$, as most sand, gravel, and clasts smaller than 0.5 m in diameter were removed from the failure mass. Much of this material was likely reworked into the beach sediments. This site was given a secondary designation, S. Newer, smaller piles of sediment were observed atop the old failure mass, the product of ongoing erosion of the unstable upper cliff. Boulders as large as ~1 m in diameter had also shifted between the surveys.

A survey performed one month after the failure indicated the slide had decreased to a volume of 37 $m^3$. The seasonal wave energy levels during this period were lower and hence unable to rework the larger clasts or reach the loose sediment sitting on top of those clasts. Minimal change was observed until about three months (~September) after the initial failure. During this latter visit, a substantial amount of vegetation and an additional 30 $m^3$ of sediment from the upper cliff had collapsed (Figure 4D). Succeeding site visits after September observed a continual increase in small amounts of sediment on top of the large clasts remaining from the first and second failures, caused by the instability of the upper slope. However, this new sediment was located too high to be reached by typical waves (Figure 9). With progress into winter and with an increase in winter waves, the resulting TWLs were found to be high enough to erode the sediment, leaving only larger clasts (> 0.3 m) on the beach.

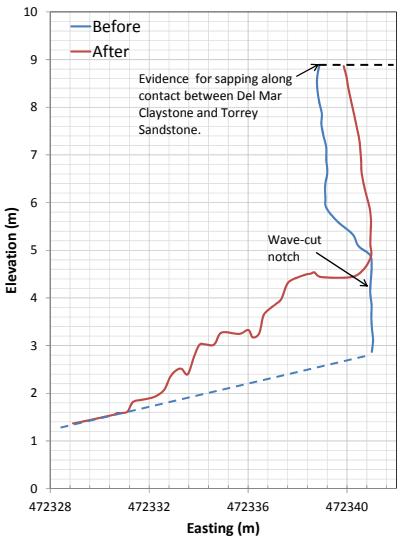


Figure 8. Cross-section of Site EN1 from lidar surveys before (April 2005) and after (June 7, 2007). Note: the upper portion of the cliff was removed because the lidar did not penetrate heavy vegetation.

**Type B Failure Sites**

**EN2**

A failure at Site EN2 (Figure 4E) was discovered during a routine visit to Site EN1 on March 7, 2008. This failure was estimated to have occurred during the end of February 2008 because the vegetation that had fallen with the failure mass was still green when surveyed in March. High water levels (from large wave events) and some precipitation occurred during this time period (Figure 5). A pronounced, wavecut notch was present at this site prior to failure. Substantial groundwater sapping is observed along the contact of the Delmar and Torrey formations as evidenced by the vegetation at the edge of the cliff, although not nearly as much vegetation as was observed at Site EN1. The failure mass was approximately 177 $m^3$ in volume when originally surveyed. Comparing the cliff from the March 2008 surveys and the October 2007 surveys yielded a volume change of approximately 200 $m^3$. A precise sediment

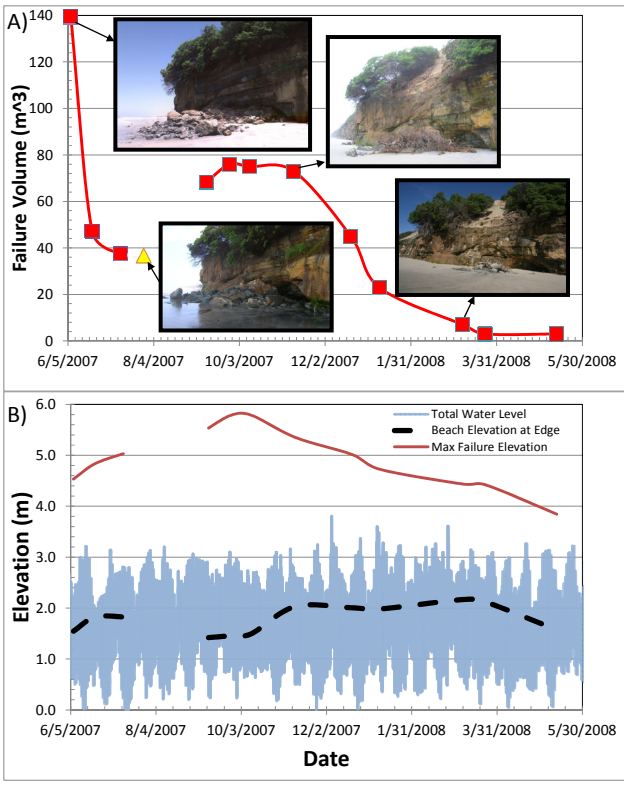


Figure 9. (A) Failure mass volume of Site EN1 with time and (B) comparison of total water level and beach elevation immediately west of failure mass. Yellow triangles indicate visits to the site where lidar surveys were not completed but the site was visually examined.

volume could not be obtained because the failure mass covered the bottom of the cliff, thus the basal shape of the cliff scar had to be inferred. The beach elevation ($E_{B0}$) was approximately 3 m on the western boundary of the failure mass when surveyed in March, so the failure mass was mostly out of the range of waves since it was first discovered.

**TP2**

Failure at Site TP2 (Figure 4I, Figure 10) occurred August 23, 2007 (+/- 1 day) on the south side of Flat Rock at Torrey Pines State Reserve. This site was of substantial concern because the failure mass landed on a pedestrian pathway used because there was no beach access during high tides. Figure 11 provides a map of the failure site at Flat Rock derived from the TLS data. Flat Rock and other exposed rocks act as barriers protecting the cliff from the waves; nevertheless, waves travelling from a direction of 245˚ and 280˚ clockwise from north will directly impact the cliff (Figure 11).

The failure mass had an original volume of 79 $m^3$. Within 20 days, the failure mass volume had dropped to 58 $m^3$. Site visits at high tide observed that waves only reached one side of the slide mass as they were blocked by exposed platforms

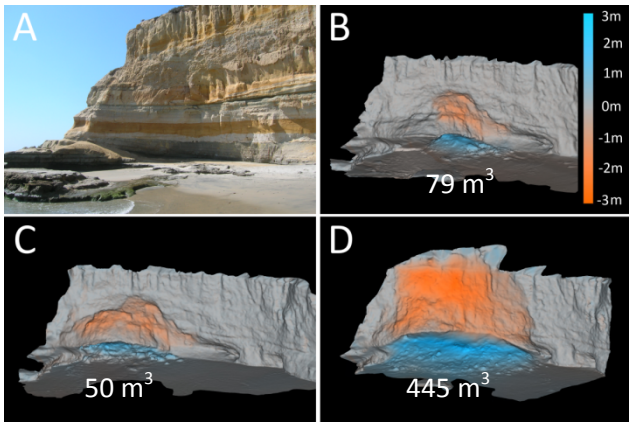


Figure 10. Comparison of Site TP2 (A) before failure (6/30/2006) and after significant failures (B) 8/23/2007 (C) 2/17/2008, and (D) 9/23/2008. All surface comparisons are relative to the survey completed on 11/3/2006.

surrounding the failure mass. A survey performed 1.5 months following the failure determined that the failure mass volume had increased to 74 $m^3$, which indicates that although the waves were eroding part of the failure mass, there was additional sediment being supplied to the failure by continued cliff erosion. This survey also observed minor movement of clasts less than 0.3 m in diameter from the waves. The beach sand levels in the small cove area in front of the failure mass increased 0.2 m during this time, and decreased by 0.5 m in the adjacent area on the north side of Flat Rock. Thus, sediment derived from the

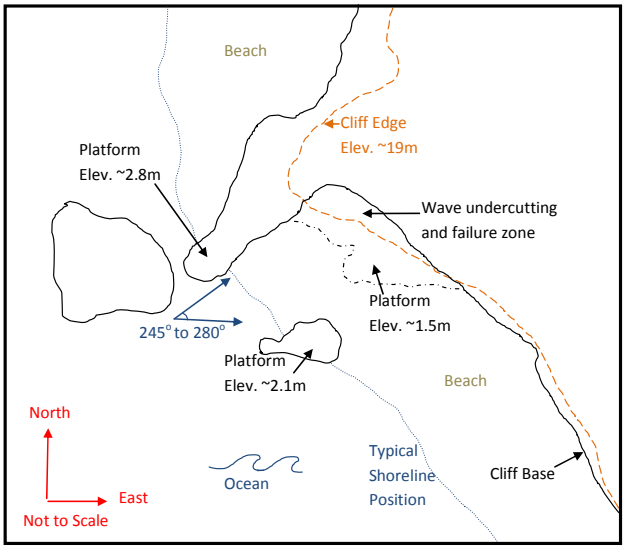


Figure 11. Map view schematic of the cliff and platform geometry for Flat Rock, Torrey Pines Reserve. Note that a peak wave direction of 245 degrees to 280 degrees measured clockwise from true North maximizes energy transfer to cliff at failure zone.

failure mass was trapped in this small cove temporarily resulting in a small amount of beach accretion. Additional clast and loose sediment accretion was commonly observed during site visits. In early February 2008, a second collapse of 50 $m^3$ occurred at this site (Figure 4J, Figure 10) during high water levels (Figure 5).

This site provides insights on the progression of instability generated in cliffs by wave undercutting and subsequent collapses of the cliff. The first collapse occurred on the lower portion of the cliff, creating a substantial overhang (Figure 4I, Figure 10). Given this unstable state, an adjacent collapse occurred (Figure 4J), engendering a larger overhang. Next, on September 21 or 22, 2008, the entire upper overhang collapsed (Figure 4K), resulting in an addition of 445 $m^3$ of material to the existing failure mass.

**TP3**

Site TP3 (Figure 4L) was first surveyed with TLS in November 2006, when a failure mass of 97 $m^3$ was observed on the beach. This failure progressed from a previous collapse of part of a column-like feature that had occurred much earlier in January 2006. By January 2007, the rest of the columnar shaped feature had collapsed on the beach and was observed to erode during the winter months. An additional collapse occurred in September 2007. Comparisons of the November 2006 survey with the October 2007 survey indicated that about 134 $m^3$ had eroded from the cliff at this site. Most of this material was dispersed and subsequently removed from the failure mass by waves, so only the largest cemented sandstone boulders remained.

**TP5**

The failure at Site TP5 (Figure 4N) occurred in January 2008 with the collapse of an overhang on the upper portion of the cliff (Figure 12) following high water levels due to increased wave activity from a storm, which resulted in about 1 cm of precipitation (Figure 5, Figure 13). Because the failure mass was directly in the reach of waves at the time of failure, it was quickly reworked along the beach (Figure 13). In addition, rising beach levels covered the larger clasts of the failure mass within a couple of months of its occurrence. Hence, because the failure occurred during the winter season when beach elevations were low, the material was quickly reworked into the beach and did not provide protection to the cliff base.

**Type C Failure Sites**

**DM2**

The failure at Site DM2 (Figure 4B) occurred in summer 2007 and was discovered during a baseline survey. Most of the failure mass was loose sand and gravel material. The failure mass volume was calculated to be 25 $m^3$ and remained constant during surveys until this sediment was quickly reworked by the increased water levels during the first winter storms in late November 2007.

**TP1**

The failure at Site TP1 (Figure 4G) occurred during the late afternoon of August 4, 2007. However, the volume of the failure mass remained constant until late December 2007 when waves eroded a protective beach berm (Figure 14) and reworked all the fine sediment from the failure mass (Figure 15). Larger clasts were pushed up against the cliff and talus deposits during winter events. Immediately to the side of these clasts and talus deposits, a smaller failure occurred in May 2008 (Figure 4H) from the collapse of an adjacent sea cave. The south edge of Site TP1 is a boundary between the talus deposits found to the north and the sea caves and wave undercutting found to the south of Torrey Pines. Additional findings of Site TP1 are presented in Olsen *et al*. (2008).

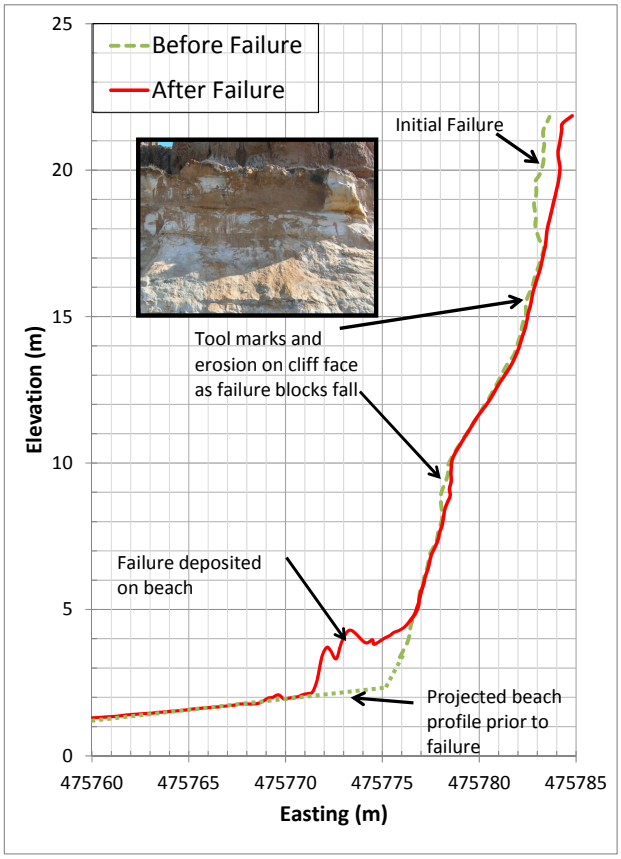


Figure 12. Cross-section of seacliff failure at Site TP5.

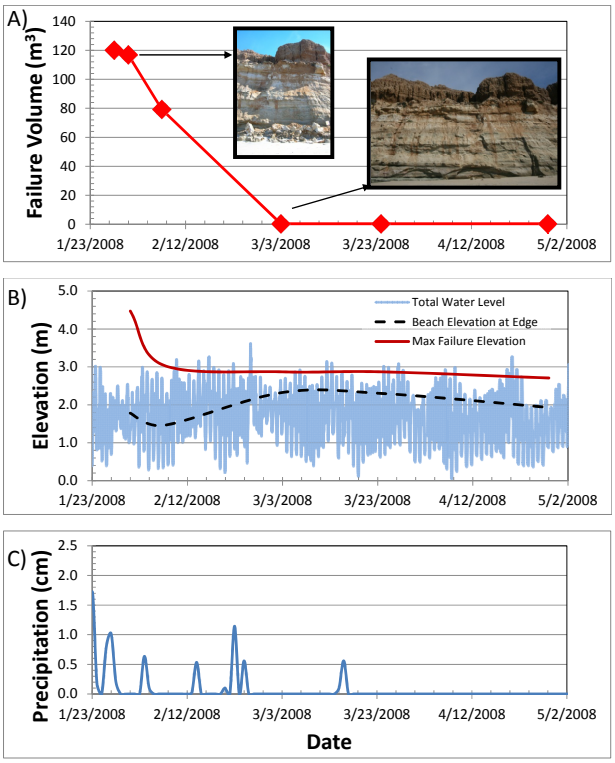


Figure 13. Analysis of failure site TP5 with (A) failure mass volume, (B) a comparison of beach height immediately west of the failure mass with the total water level, and (C) precipitation levels.

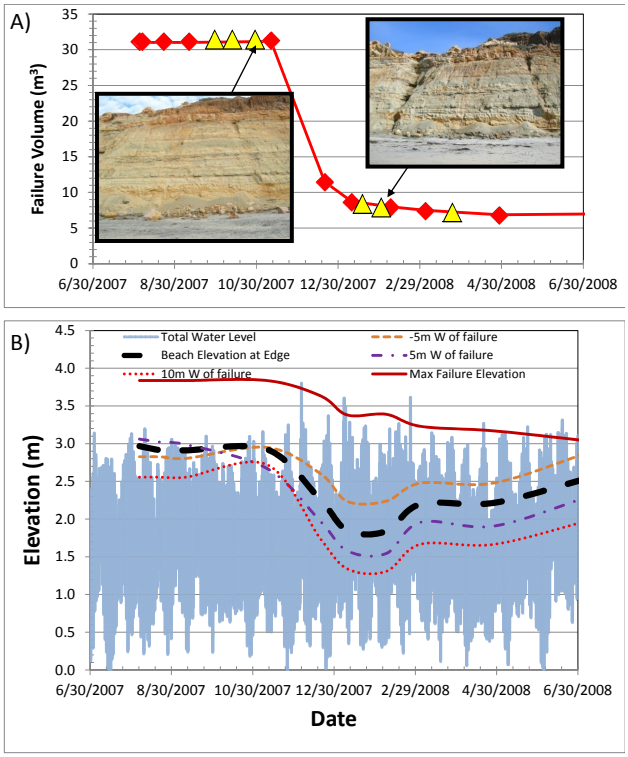


Figure 15. (A) Failure mass volumetric change analysis and (B) comparison of beach sand levels to TWL for Site TP1. Red diamonds represent TLS surveys and yellow triangles represent field visits.

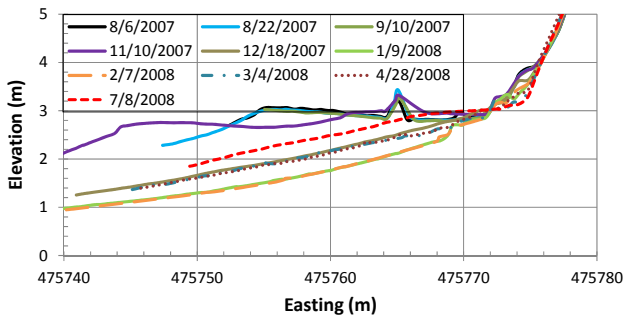


Figure 14. Beach profiles at Site TP1 from TLS data. Note rapid erosion of beach berm between 11/10/2007 and 12/20/2007 with initial winter storms.

**TP4**

This failure (Figure 4M) occurred on approximately October 20, 2007, during a storm event with precipitation and some minor wave activity (Figure 5). The failure mass landed on a beach berm where high water levels were able to reach the base of the failure mass periodically. The failure occurred on the upper portion of the cliff (Figure 16). Falling debris impacted the top of the talus deposits, resulting in a small loss of material in the top of the talus deposits. As soon as water levels increased during the winter months, waves reached the failure mass and much of the failure material was quickly eroded (Figure 17).

Analyzing the cross-sections (Figure 18) of the beach and talus deposits at this site indicates that after the initial waves reworked the finer sediment from the failure mass, the larger failure boulders (>0.5 m in diameter) were pushed up against the talus deposits and acted as a protection to the cliff toe, similar to riprap stabilization techniques. Furthermore, the failure material behaved as a sediment trap, collecting talus deposits behind it that would otherwise land on the beach and be quickly reworked (Figure 18). Examining the seacliff profiles on either side of the failure mass revealed that substantial erosion of talus deposits occurred during the winter, leaving the cliffs exposed to wave attack (Figure 19).

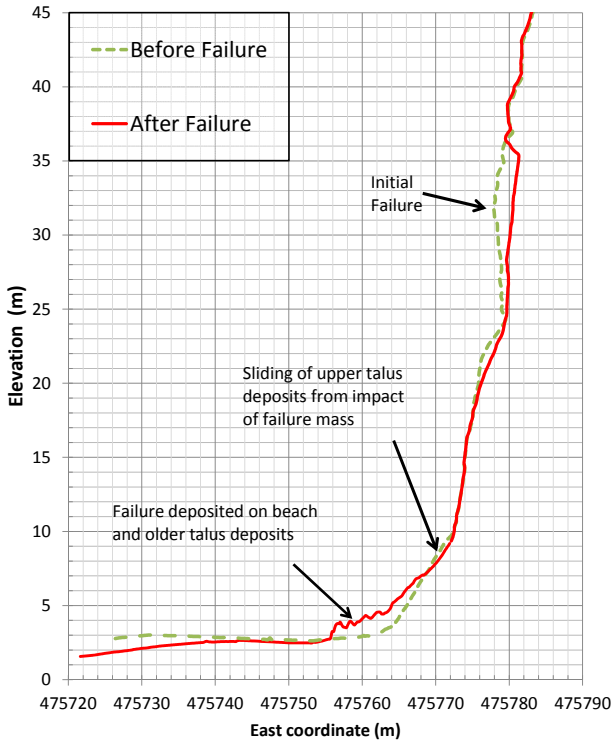


Figure 16. Cross-section analysis of failure at Site TP4.

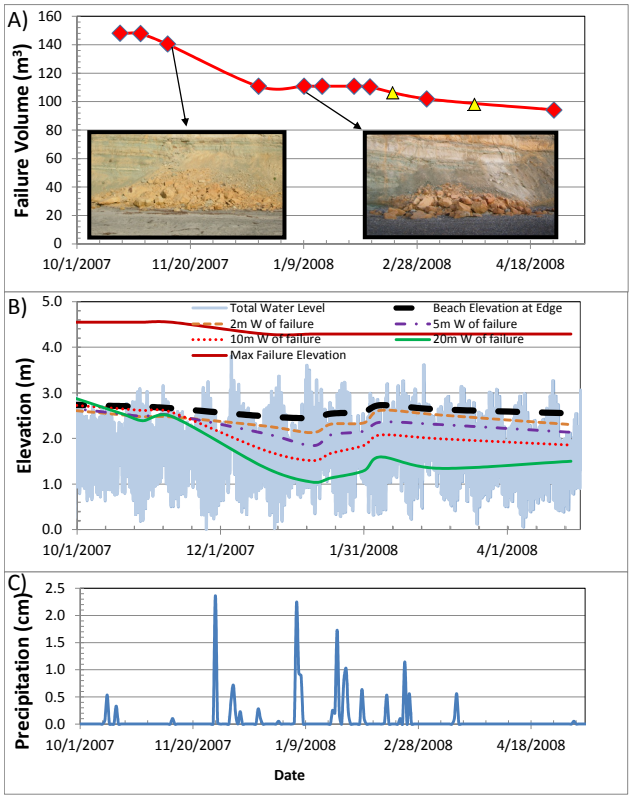


Figure 17. Comparison of (A) failure mass volume determined from TLS, (B) beach elevation and total water level, and (C) precipitation for Site TP4. Red diamonds represent TLS surveys and yellow triangles represent field visits.

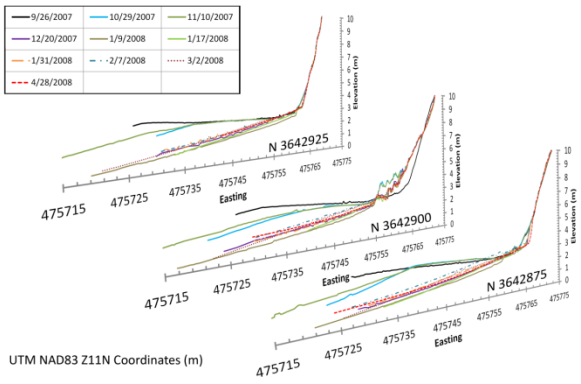


Figure 18. Comparison of beach and talus deposit profiles for Site TP4, which experienced increased erosion of talus deposits 25 m to the north and south of the failure site and protection of talus deposits at the failure site.

**TP6**

The failure at Site TP6 (Figure 4O) occurred in June 2008 on the unstable upper cliff (Figure 20). Several tree roots have created joints in the sandstone and provide strong evidence for biological weathering. The vegetation also implies the presence of some groundwater in the sandstone; however, no sapping was observed. Subsequent monitoring of erosional processes at this site is described in more detail in Johnstone *et al*. (2016).

**Type D Failure Sites**

**DM1**

The failure at Site DM1 (Figure 4A) occurred in mid-August 2007 in an unstable area undergoing a substantial amount of erosion due to groundwater sapping and surface runoff from a storm drain. Previous failures at this location are discussed in Young and Ashford (2007). Repeat scans captured minimal change in the failure mass volume (88 $m^3$) at the site because the majority of the failure mass rests on a shore platform.

**SIO1**

This 30 $m^3$ failure (Figure 4F) occurred approximately 250 m north of the pier at Scripps Institution of Oceanography in September 2007 and was deposited on a shore platform located at an elevation of ~3 m. Some undercutting had previously occurred above the platform (Figure 21). Waves generally were unable to reach the failure material because of its perched

position, resulting in minimal change in the failure mass. During precipitation events, a small amount (< 1 $m^3$) of the failure mass was washed off the platform. During the winter season, approximately 8 $m^3$ of sediment was eventually removed from the failure mass, most of which was in the center of the failure mass where the platform does not extend as far seaward.

## DISCUSSION

This study places important new constraints on wave reworking rates of cliff failure material. Failure sites (Types A, B, and C) that are exposed to waves experienced rapid removal of sediment, the product of high wave runup. Type A sites (EN1) suggest that even lower energy summer waves are sufficient to rework loose sediment and smaller clasts from the failure mass. Conversely, Type B sites (*e.g.*, TP5) allow waves occurring at higher water levels to quickly entrain and redistribute the sediment elsewhere. Most other sites (Type C, *e.g.*, TP1, TP4, and DM1) required very high water levels from high tides or major storms to reach the failure mass volume or erode a protective beach berm. Type D failures exhibited minimal loss of sediment and only would be reworked during the largest of storm events, which did not occur during the study period. As discussed in Young and Ashford (2007), several small seacliff failures can account for a significant portion of the sediment contributed to the beach. Hence, this study suggests that sediment derived from failures requires minimal wave energy to rework and entrain the sediment, and do contribute significant portions of sand to the beach system.

For instance, Sites TP1 and TP4 (Type C) both had a large beach berm that was only slightly eroded during the start of the winter season. As soon as water levels increased as major winter storms hit in late November and December, the waves quickly reworked and eroded the beach berm. Interestingly, some sites (Types A and B) that did not have a beach berm (EN1, TP5) experienced a detectable increase in beach elevation during the winter months, probably as a result of sediment being redistributed from sites with large sediment supply to sites with less sediment from the high-energy winter waves.

Furthermore, insights into beach system dynamics were also uncovered by the heightened temporal resolution of this study, where seasonal beach accretion and removal is asymmetric. Summer beach sand levels change rapidly with the onset of the first major winter storms, eroding the beach berm within a matter of a few weeks. In contrast, the summer build-up of sediment is much more gradual, occurring over a period of a few months.

This study also further documents that talus deposits play a significant role in the style of cliff erosion since they provide protection of the cliff base. For the Torrey Pines section (Figure 1), a demarcation line between sections with Talus and those without occurs immediately to the south of Site TP1. Type C failures occurred in locations to the north where talus deposits were present to protect the seacliffs from wave-induced erosion. Sediments were slower to rework into the beach. To the south, sea caves and wave undercutting are much more dominant because of the lack of talus deposits protecting the cliffs. Type B failures were commonly observed in this section and likely occurred from wave-induced erosion. Sediments at these sites were reworked faster into the beach.\

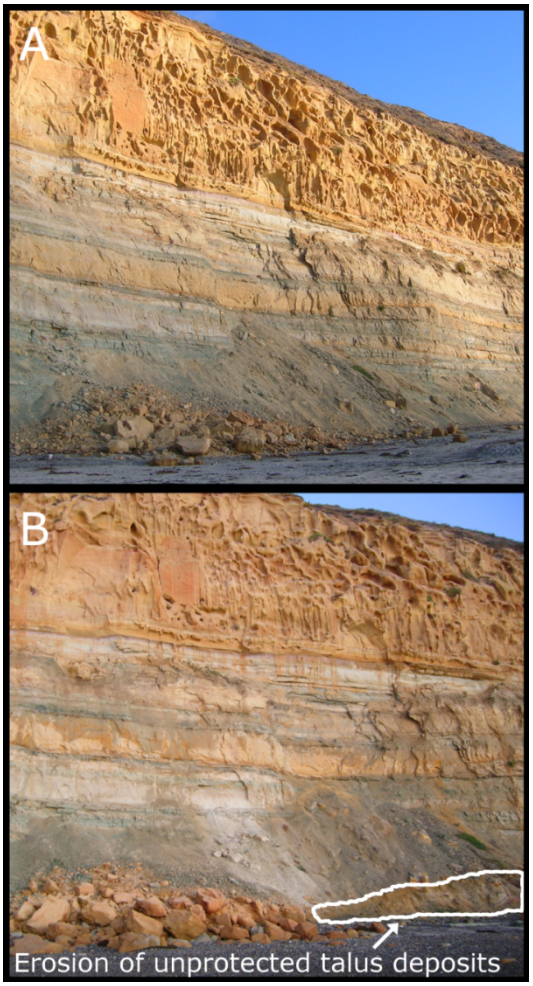


Figure 19. Failure Site TP4 (A) before (November 11, 2007) and (B) after (January 9, 2008) winter storms. Note the failure mass stabilizing talus deposits while talus deposits away from the failure mass experienced substantial erosion.

In addition to the protection offered by talus deposits, a failure mass can act as riprap stabilization and minimize local cliff erosion, provided the failure material consists of large boulders that trap talus deposits while erosion continues to occur adjacent to the failure mass. Smaller clasts from the failure mass can be hurled by waves at the adjacent cliff; these tools accelerate the wave-induced erosion. The failed sediment also can cause abrasion on the unprotected cliff. Site TP4 (Type C) provides a clear example of this phenomenon, where talus deposits grew slightly near the failure mass during the winter months, protecting the cliff toe from additional wave erosion and undercutting. The mild winter did not have substantial wave

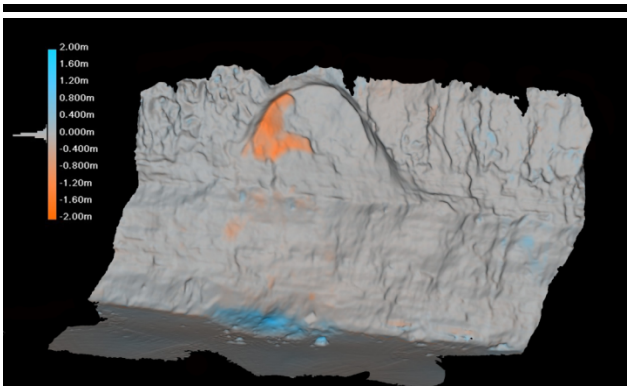


Figure 20. Surface change analysis for Site TP6 comparing the post-failure, June 18, 2008, survey to the pre-failure, April 28, 2008, survey.

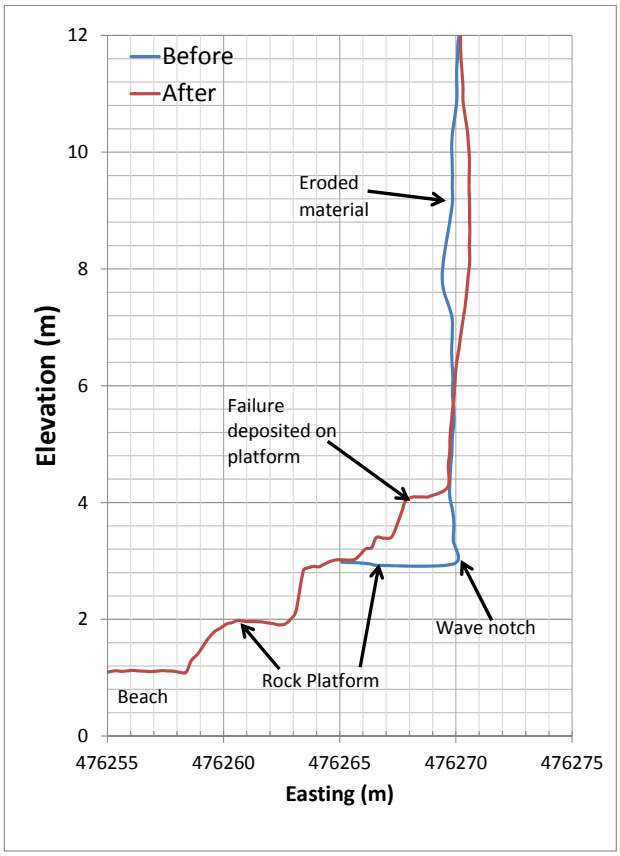


Figure 21. Cross-section analysis for Site SIO1 with a failure mass atop the rock platform.

energy to rework and transport the large boulders. In contrast, talus deposits adjacent to the failure mass were eroded and exposed the cliff to ongoing wave activity during the winter months (Figures 18 and 19). After February 2008, beach levels began to increase and bury portions of the failure mass (Figure 17).

Site TP1 also exhibited similar behavior to Site TP4 where the talus deposits at the site of the failure mass remain in place during the winter because of the larger stabilizing clasts. At the edges of the failure mass, however, wave energy still managed to contribute to the collapse of a sea cave (Figure 4H). In contrast, at Site TP2 (Type B, no talus deposits), a second failure occurred adjacent to the first failure as wave energy was concentrated on either side of the initial failure mass. The importance of talus deposits in protecting the cliffs from wave-induced erosion is illustrated by the fact that wave undercutting and undercutting only occurred at sites without talus deposits (Table 1). This phenomenon may be important in understanding the influence of sea level rise on cliff erosion, such that the talus may protect some sections of the cliff while accelerating erosion and undercutting along the adjacent cliff section. This may provide a nucleation site and feedback that acts to cause cliff erosion and undercutting to radiate out away from regions with failed material on the beach.

In addition to serving as talus stabilization, boulders in failure masses that occur in areas subject to dynamic beach change can directly contribute to increased beach volume. This is another feedback mechanism that slows erosion for two reasons. First, higher beach elevations cover more of the cliff base and prevent water from reaching the base of the cliff. Second, when the beach progresses towards the ocean, more wave energy is dispersed along the beach prior to reaching the cliff. During winter storms, the sand from the failure mass is eroded, leaving the boulders perched on the beach. However, with a return to summer, the waves do not have sufficient power to rework or move the large boulders. Thus, the returning sand is deposited on top of and around the old boulders. During winter, the boulders are then re-exposed and can act as either protective or destructive mechanisms depending on the wave energy, boulder size, and their geometrical arrangement, as was observed at sites EN1 and TP5.

## CONCLUSIONS

TLS provides a valuable tool to understand and quantify geologic processes using efficient, high-resolution spatial and temporal surveys. Comparing the TLS data with available environmental data enables us to assess various triggering mechanisms for seacliff failures. Several failures occurred in association with high water levels associated with increased wave activity from storm events. Frequent site observations and repeated mapping following a collapse provides new insights on sediment reworking processes. First, minimal wave energy is required to rework unconsolidated failure masses into the beach system. Thus, seemingly small erosion over the entire cliff face is rapidly absorbed by the physical system, such that it is continually supplying material to the beach system. Second, feedback mechanisms occur from seacliff failure masses, protecting the cliff directly behind the failure mass and accelerating erosion to adjacent areas next to the failure mass (*e.g.*, at Site TP4). The increased material also directly contributes to beach building, which can further help protect the cliff toe. These new insights gleaned from quantitative, time-series data indicate dominant wave undercutting and subordinate

subaerial processes lead to the long-term spatially linear fashion of seacliff retreat with minimal irregularities. Third, most sand on the beach is removed rapidly during the first winter storms and then is gradually replaced on the beach during the lower energy summer months. These observations highlight the importance of seacliff erosion in providing sand and stabilization to beaches. Finally, the classification system developed in this paper can assist with the prioritization of study sites for repeat surveys and provides insights on the failure mechanisms where Type A and B failures tend to be wave-induced and Type C and D failures tend to be subaerial.

## ACKNOWLEDGMENTS

This research was supported by California Seagrant (Project #R/OE-39) and the Coastal Environmental Quality Initiative (CEQI) under award #04-T-CEQI-06-0046. We would like to thank Pat Rentz and Jessica Raymond for their assistance in the TLS surveys, Gary Samad for alerting us to the locations of several cliff failures, and Adam Young for providing the 2005 scans of Site EN1 and assisting in a survey of Site EN1. Scott Schiele and John Dolan from Maptek I-Site provided technical assistance for this work. Travis Thompson provided technical assistance with the CALVRS GPS network. We thank the anonymous reviewers for their detailed review and suggestions, which helped improve the manuscript.

## LITERATURE CITED

Benumof, B.T.; Storlazzi C.D.; Griggs G.B., and Seymour R.J., 2000. The relationship between incident wave energy and seacliff erosion rates: San Diego County, California. *Journal of Coastal Research*, 16(4), 1162–1178.

Collins, B. and Sitar, N., 2004. Application of high resolution 3d laser scanning to slope stability studies. *Proceedings of the 39th Annual Symposium on Engineering Geology and Geotechnical Engineering* (Butte, MT), pp. 79–92.

Collins, B.; Kayen, R.; Reiss, T., and Sitar, N., 2007. *Terrestrial lidar investigation of the December 2003 and January 2007 activations of the Northridge Bluff Landslide, Daly City, California. U.S. Geologic Survey Open-File Report 2007-1079*, 32p.

Dong, P. and Guzzetti, F., 2005. Frequency-size statistics of coastal soft cliff erosion. *Journal of Waterway, Port, Coastal, and Ocean Engineering*, 131(1), 37–42.

Everts, C.H., 1990. Sediment Budget Report Oceanside Littoral Cell. U.S. Army Corp of Engineers, Los Angeles District, Coast of California Storm and Tidal Wave Study, 90(2), 110p.

Griggs, G.B.; Patsch, K., and Savoy, L.E., 2005. *Living With the Changing California Coast*. Berkeley: University of California Press, 540p.

Haas, J., 2005. Grain Size and Mineralogical Characteristics of Beach Sand with Implications for Sediment Provenance in the Oceanside Littoral Cell. San Diego, California: University of California, San Diego, Master's thesis, 126p.

Hapke, C. and Richmond, B., 2000. Monitoring beach morphology changes using small-format aerial photography and digital softcopy photogrammetry. *Environmental Geosciences*, Special Issue on Coastal Hazard Mapping Techniques, 7(1), 32–37.

I-Site, 2009. Maptek I-Site Studio Software. http://www.isite3d.com.

Kennedy, M.P., 1973. Bedrock Lithologies, San Diego Coastal Area, California. *In*: Ross, A. and Dowlen, R.J. (eds.), *Studies on the Geology and Geologic Hazards of the Greater San Diego Area, California*. San Diego: San Diego Geological Society, pp. 9–15.

Kennedy, M.P., 2005. Geologic Map of the San Diego 30' x 60' Quadrangle, California. California Department of Conservatism.

Johnstone, E.; Raymond, J.; Olsen, M.J., and Driscoll, N., 2016. Morphological expressions of coastal cliff erosion processes in San Diego County. *In*: Brock, J.C.; Parrish, C.E.; Gesch, D.; Wright, C.W., and Rogers, J. (eds.), *Advances in Topobathymetric Mapping, Models, and Applications. Journal of Coastal Research*, Special Issue, No. 76, pp. 174–184.

Lim, M.; Petley, D.N.; Rosser, N.J.; Allison, R.J., and Long, A.J., 2005. Combined digital photogrammetry and time-of-flight laser scanning for monitoring cliff evolution. *The Photogrammetric Record*, 20(110), 109–129.

Moore, L.J.; Benumof, B., and Griggs, G.B., 1999. Coastal erosion hazards in Santa Cruz and San Diego Counties, California. *In*: Crowell, M. and Leatherman, S.P. (eds.), *Coastal Erosion Mapping and Management*. *Journal of Coastal Research*, Special Issue, No. 28, pp. 121–139.

National Oceanographic and Atmospheric Administration, NOAA, 2008a. National Climatic Data Center (NCDC). http://www.ncdc.noaa.gov/oa/ncdc.html.

National Oceanographic and Atmospheric Administration, NOAA, 2008b. NOAA Tides and Currents. http://tidesandcurrents.noaa.gov.

Olsen, M.J.; Johnstone, L.; Young, A.P.; Hsieh, T.J.; Ashford, S.A.; Driscoll, N., and Kuester, F., 2008. Rapid response to seacliff erosion in San Diego County using terrestrial lidar. *Proceedings, Solutions to Coastal Disasters Conference* (Oahu, Hawaii, ASCE), pp. 573–583.

Olsen, M.J., 2009. Methodologies for Assessing Coastal Change Using Terrestrial Laser Scanning. San Diego, California: University of California, San Diego, Ph.D. Dissertation, 267p.

Olsen, M.J.; Johnstone, E.; Driscoll, N.; Ashford, S.A., and Kuester, F., 2009. Terrestrial laser scanning of extended cliff sections in dynamic environments: Parameter analysis. *Journal of Surveying Engineering*, 135(4), 161–169.

Olsen, M.J.; Johnstone, E.; Kuester, F.; Driscoll, N., and Ashford, S.A., 2011. New automated point-cloud alignment for ground-based light detection and ranging data of long coastal sections. *Journal of Surveying Engineering*, 137(1), 14–25.

Olsen, M.J.; Johnstone E., and Kuester F., 2013. Hinged, pseudo-grid triangulation method for long, near linear cliff analysis. *Journal of Surveying Engineering*, 139(2), 105–109.

Rosser, N.J.; Petlety, D.N.; Lim, M.; Dunning, S.A., and Allison, R.J., 2005. Terrestrial laser scanning for monitoring the process of hard rock coastal cliff erosion. *Quarterly Journal of Engineering Geology and Hydrology*, 38, 363–375.

Rosser, N.J.; Lim, M.; Norman, E., and Petley, D.N., 2008. Exploring variations in and controls upon cliff, platform and coastline geometry. *European Geosciences Union Geophysical Research Abstracts*, 10, EGU2008-A-10318.

Ruggiero, P.; Komar, P.D.; McDougal, W.G., and Beach R.A., 1996. Extreme water levels, wave run-up, and coastal erosion. *Proceedings of the 25th Coastal Engineering Conference* (Orlando, Florida, ASCE), pp. 2793–2805.

Ruggiero, P.; Komar, P.D.; McDougal, W.G.; Mara, J.J., and Beach, R.A., 2001. Wave run-up, extreme water levels and he erosion of properties backing beaches. *Journal of Coastal Research*, 17(2), 407–419.

Ruggiero, P., 2008. Impacts of climate change on coastal erosion and flood probability in the Pacific Northwest. *Proceedings of the Solutions to Coastal Disasters Conference* (Oahu, Hawaii, ASCE), pp. 158–169.

Scripps Institution of Oceanography, 2008. The Coastal Data Information Program (CDIP). Integrative Oceanography Division, Scripps Institution of Oceanography, San Diego. http://cdip.ucsd.edu.

Stockdon, H.F.; Holman, R.A.; Howd, P.A., and Sallenger, A.H., 2006. Empirical parameterization of setup, swash, and run-up. *Coastal Engineering*, 53(7), 573–588.

Sunamura, T., 1992. *Geomorphology of Rocky Coasts*. New York: John Wiley and Sons, 302p.

Weissel, J.K. and Driscoll, N.W., 1998. Landslides: An onshore-offshore comparison. AGU 1998 Fall Meeting, H32G-06.

Wolters, G. and Muller, G., 2008. Effect of cliff shape on internal stresses and rock slope stability. *Journal of Coastal Research*, 24(1), 43–50. ISSN 0749-0208.

Young, A.P. and Ashford, S.A., 2006. Application of airborne lidar for seacliff volumetric change and beach sediment budget contributions. *Journal of Coastal Research*, 22(2), 307–318.

Young, A.P. and Ashford, S.A., 2007. Quantifying sub-regional seacliff erosion using mobile terrestrial lidar. *Shore and Beach*, 75(3), 38–43.

Young, A.P.; Guza, R.T.; Flick, R.E.; O'Reilly, W.C., and Gutierrez, R., 2009. Rain, waves, and short-term evolution of composite seacliffs in southern California. *Marine Geology*, 267(1–2), 1–7.

Young, A.P.; Olsen, M.J.; Driscoll, N.; Flick, R.E.; Gutierrez, R.; Guza, R.T.; Johnstone, E., and Kuester, F., 2010a. Comparison of airborne and terrestrial lidar estimates of seacliff erosion in Southern California. *Photogrammetric Engineering and Remote Sensing*, 76(4), 421–427.

Young, A.P.; Raymond, J.H.; Sorenson, J.; Johnstone, E.A.; Driscoll, N.W.; Flick, R.E., and Guza, R.T., 2010b. Coarse sediment yields from seacliff erosion in the Oceanside Littoral Cell. *Journal of Coastal Research*, 26(3), 580–585.